

Discovery of a magnetar candidate X-ray pulsar in the Large Magellanic Cloud[★]

M. Imbrogno,^{1,2,†} G. L. Israel,² G. A. Rodríguez Castillo,³ D. A. H. Buckley,^{4,5} F. Coti Zelati,^{6,7} N. Rea,^{6,7} I. M. Monageng,^{4,5} P. Casella,² L. Stella,² F. Haberl,⁸ P. Esposito,^{9,10} F. Tombesi,^{1,2,11,12,13} A. De Luca,¹⁰ and A. Tiengo^{9,10}

¹Dipartimento di Fisica, Università degli Studi di Roma “Tor Vergata”, via della Ricerca Scientifica 1, I-00133 Rome, Italy

²INAF–Osservatorio Astronomico di Roma, via Frascati 33, I-00078 Monteporzio Catone, Italy

³INAF/IASF Palermo, via Ugo La Malfa 153, I-90146 Palermo, Italy

⁴South African Astronomical Observatory, PO Box 9, Observatory, Cape Town 7935, South Africa

⁵Department of Astronomy, University of Cape Town, Private Bag X3, 7701 Rondebosch, South Africa

⁶Institute of Space Sciences (ICE, CSIC), Campus UAB, Carrer de Can Magrans s/n, E-08193 Barcelona, Spain

⁷Institut d’Estudis Espacials de Catalunya (IEEC), Carrer Gran Capità 2–4, E-08034 Barcelona, Spain

⁸Max-Planck-Institut für extraterrestrische Physik, Gießenbachstraße 1, 85748 Garching, Germany

⁹Scuola Universitaria Superiore IUSS Pavia, Palazzo del Broletto, piazza della Vittoria 15, I-27100 Pavia, Italy

¹⁰INAF/IASF Milano, via A. Corti 12, I-20133 Milan, Italy

¹¹Department of Astronomy, University of Maryland, College Park, MD 20742, USA

¹²NASA Goddard Space Flight Center, Greenbelt, MD 20771, USA

¹³INFN – Roma Tor Vergata, via della Ricerca Scientifica 1, I-00133 Rome, Italy

Accepted XXX. Received YYY; in original form ZZZ

ABSTRACT

During a systematic search for new X-ray pulsators in the *XMM-Newton* archive, we discovered a high amplitude ($PF \approx 86\%$) periodic ($P \approx 7.25$ s) modulation in the X-ray flux of 4XMM J045626.3-694723 (J0456 hereafter), a previously unclassified source in the Large Magellanic Cloud (LMC). The period of the modulation is strongly suggestive of a spinning neutron star (NS). The source was detected only during one out of six observations in 2018–2022. Based on an absorbed power-law spectral model with photon slope of $\Gamma \approx 1.9$, we derive a 0.3–10 keV luminosity of $L_X \approx 2.7 \times 10^{34}$ erg s⁻¹ for a distance of 50 kpc. The X-ray properties of J0456 are at variance with those of variable LMC X-ray pulsars hosted in high-mass X-ray binary systems with a Be-star companion. Based on *SALT* spectroscopic observations of the only optical object that matches the X-ray uncertainty region, we cannot completely rule out that J0456 is a NS accreting from a late-type (G8–K3) star, an as-yet-unobserved binary evolutionary outcome in the MCs. We show that the source properties are in better agreement with those of magnetars. J0456 may thus be second known magnetar in the LMC after SGR 0526–66.

Key words: stars: neutron – galaxies: individuals: Large Magellanic Cloud

1 INTRODUCTION

The Small and Large Magellanic Clouds (SMC and LMC, respectively) are the two best-studied star-forming satellite galaxies of the Milky Way. Thanks to their recent star formation bursts (in the inner regions) occurred ~ 6 –25 Myr ago in the LMC and ~ 25 –60 Myr ago in the SMC (Antoniou et al. 2010; Antoniou & Zezas 2016), the MCs host a high number of X-ray pulsars, neutron stars (NSs) emitting in the X-ray band and showing coherent pulsations originated by the NS rotation around its axis. In particular, the MCs host an unusu-

ally high number of High Mass X-ray binaries (HMXBs), systems in which the compact object, a NS or a black hole (BH), orbits an early (spectral type O/B) companion.

BeXRBs (HMXBs with a bright Be spectral-type companion; see Coe 2000; Okazaki & Negueruela 2001 for a review) represent the most numerous subclass of HMXBs in the MCs, with ~ 150 BeXRBs out of ~ 160 HMXBs. A total of ~ 80 BeXRBs, in particular, host X-ray pulsars (Coe & Kirk 2015; Antoniou & Zezas 2016; Haberl & Sturm 2016; Haberl et al. 2022b). The recent discoveries of new HMXBs and pulsars in BeXRBs in the outskirts of the LMC suggest that more systems are likely hidden in these regions (Vasilopoulos et al. 2018; Maitra et al. 2021; Haberl et al. 2022b; Maitra et al. 2023). Only one Low Mass X-ray Binary (LMXB, i.e. XRB whose companion has a mass $M \lesssim 1 M_\odot$) hosting an accreting NS is known in the LMC, namely LMC X-2. The source is persistent and shows ther-

[★] Based on observations obtained with XMM-Newton, an ESA science mission with instruments and contributions directly funded by ESA Member States and NASA.

[†] E-mail: matteo.imbrogno@inaf.it

monuclear bursts, testifying to the presence of an old/low-magnetic field strength NS. No coherent or quasi-coherent periodic signals have been reported for LMC X-2 (see [Agrawal & Nandi 2020](#), and reference therein).

The SMC and the LMC are also known to host two magnetars, CXOU J010043.1–721134 ([Lamb et al. 2002, 2003; McGarry et al. 2005; Tiengo et al. 2008; Chatterjee et al. 2021](#)) and SGR 0526–66 ([Mazets et al. 1979; Kulkarni et al. 2003; Tiengo et al. 2009; Park et al. 2020](#)) respectively. Magnetars ([Duncan & Thompson 1992](#)) are isolated NSs whose emission is (in the majority of the cases) in excess of their spin-down luminosities. Their emission is thought to be powered (for the most part) by the release of energy by the strong ($10^{14} \text{ G} \lesssim B \lesssim 10^{16} \text{ G}$) magnetic fields in their interior (for recent reviews, see [Turolla et al. 2015; Kaspi & Beloborodov 2017; Esposito et al. 2021](#)). Currently, about 30 magnetars are known, all in our Galaxy with the exception of the two magnetars in the MCs.

In this paper, we report on the discovery of X-ray pulsations at a period of about 7.25 s from a serendipitous source in the outskirts of the LMC, namely 4XMM J045626.3–694723 (J0456 henceforth). Although an unambiguous classification is still missing, the discovery of the 7.25-s periodicity that we report in this paper is strongly suggestive of a spinning NS. We discuss two competing scenarios capable of accounting for the source’s observed properties: an accreting NS hosted in a very rare evolutionary outcome for an XRB or an isolated NS belonging to the magnetar class. In the latter case, J0456 would represent the third known magnetar in the MCs.

The article is structured as follows: in Sect. 2 we describe the observations analysed in this article and the data processing techniques that we applied. In Sect. 3, we report on the results of our timing and spectral analyses. We discuss our results and the possible nature of this newly discovered pulsar in Sect. 4. Our conclusions are in Sect. 5.

2 OBSERVATIONS AND DATA REDUCTION

2.1 X-ray observations

J0456 is located in an outer region of the LMC that has been observed twice by *XMM-Newton* ([Jansen et al. 2001](#)). The source was detected only during the second pointing (obs. 0841660501, duration $T \approx 47$ ks) in October 2019. EPIC PN ([Strüder et al. 2001](#)) and EPIC MOS1 and MOS2 ([Turner et al. 2001](#)) data are available. The source was clearly detected in the three CCD cameras, which were operating in Full Frame mode (time resolution of 73.4 ms for EPIC PN, 2.7 s for EPIC MOS1 and 2.6 s for EPIC MOS2). We used *sas* ([Gabriel et al. 2004](#)) v.20.0.0 and standard data reduction procedures to prepare the raw data for timing and spectral analysis. For the PN data, we considered only events with PATTERN ≤ 4 , while for MOS data we selected events with PATTERN ≤ 12 . Since J0456 was observed near the border of a PN chip gap, we selected events for both timing and spectral analyses in a 14×8 arcsec elliptical region aligned with the chip border and centred on the source position RA = $4^{\text{h}}56^{\text{m}}26^{\text{s}}.36$, Dec = $-69^{\circ}47'23''$. The background was evaluated using a large source-free circular region on the same chip with radius 80 arcsec. The same regions were considered for the MOS cameras. The event arrival times were converted to the barycentre of the Solar System using the *sas* task BARYCEN and the source position. Response matrices and ancillary files were produced using the *sas* tasks RMFGEN and ARFGEN, respectively. For our X-ray timing and spectral analyses we considered events in the 0.3–10 keV band. Unless otherwise stated, the reported errors correspond to 1σ (68.3%) confidence ranges. A total of 776 events (source+background) were

collected by the PN (426) and MOSs (350) cameras in the source extraction region, corresponding to a background-subtracted count rate of $(2.71 \pm 0.09) \times 10^{-3}$ count/s.

No pointings covering the source position are present in the *Chandra* and *NuSTAR* archives. 20 *Swift* pointings are found, though the XRT throughput and the relatively short exposures provided poor constraints (see Sect. 3.2 for more details). Two *RXTE* pointings were found and considered in the timing analysis (see Sect. 3.1).

Finally, *eROSITA* ([Predehl et al. 2021](#)) observed the field of J0456 during the all-sky surveys but the source was always too faint to be detected. Most of our analyses are based on the *XMM-Newton* observation 0841660501 during which the source was detected. The left panel in Fig. 1 shows a close-up view of J0456 field as observed by *XMM-Newton* during this observation, together with the extraction region of the source events (highlighted in red).

2.2 Optical observations

Following [Kirsch et al. \(2004\)](#) and [Webb et al. \(2020\)](#), we adopted a 2 arcsec uncertainty radius at 3σ confidence level for the positional accuracy. Within the *XMM-Newton* uncertainty region of J0456 we identified only one possible optical counterpart in the *Gaia* DR3 catalogue ([Prusti et al. 2016; Gaia Collaboration et al. 2022](#)), with a magnitude $G \sim 19.2$ mag. We observed this source with the 11-m Southern African Large Telescope *SALT* ([Buckley et al. 2006](#)) during two consecutive nights, on November 24, 2022 and November 25, 2022. The right panel in Fig. 1 shows a close-up view of J0456 field as observed by *SALT* on November 24, 2022, together with the 3σ uncertainty region of J0456 (highlighted in red). The observations were divided in 5×1200 s exposures, for a total of 6000 s. During both nights the seeing was ~ 2 arcsec with clear sky condition. We used the Robert Stobie Spectrograph RSS ([Burgh et al. 2003; Kobulnicky et al. 2003](#)) in long-slit spectroscopy mode for a spectral classification of the source. The PG0700 grating was used with a tilt angle of 4.6° , which resulted in a wavelength range of 3600 – 7400 Å. The primary reductions, which include overscan corrections, bias subtraction, gain and amplifier cross-talk corrections, were performed with the *SALT* science pipeline ([Crawford et al. 2012](#)). The remaining steps, including wavelength calibration, background subtraction and extraction of the one-dimensional spectra were performed with *IRAF*. The spectrophotometric standard star, LTT1788, was observed with the same grating settings as our target with an exposure time of 60 s. The reduction of the spectrum of LTT1788 was performed using the same procedure described above and a relative flux calibration was applied to our target spectrum.

3 RESULTS

3.1 Timing Analysis

Pulsations from J0456 were first detected within the framework of an extension of the Exploring the X-ray Transient and variable Sky (EXTraS) project¹ ([De Luca et al. 2021, Rodríguez Castillo et al., in prep.](#)). We started from the EXTraS discovery parameters: a peak at a frequency $\nu \approx 0.138$ Hz in the PN data with a confidence level of about 5.6σ . We followed [Israel & Stella \(1996\)](#) to infer the significance of the peak and the detection threshold in the PSD. As reported above, the vicinity of the source to the CCD gap motivated

¹ The details of the periodic signal-search pipeline can be found in Sect. 4 of [De Luca et al. \(2021\)](#).

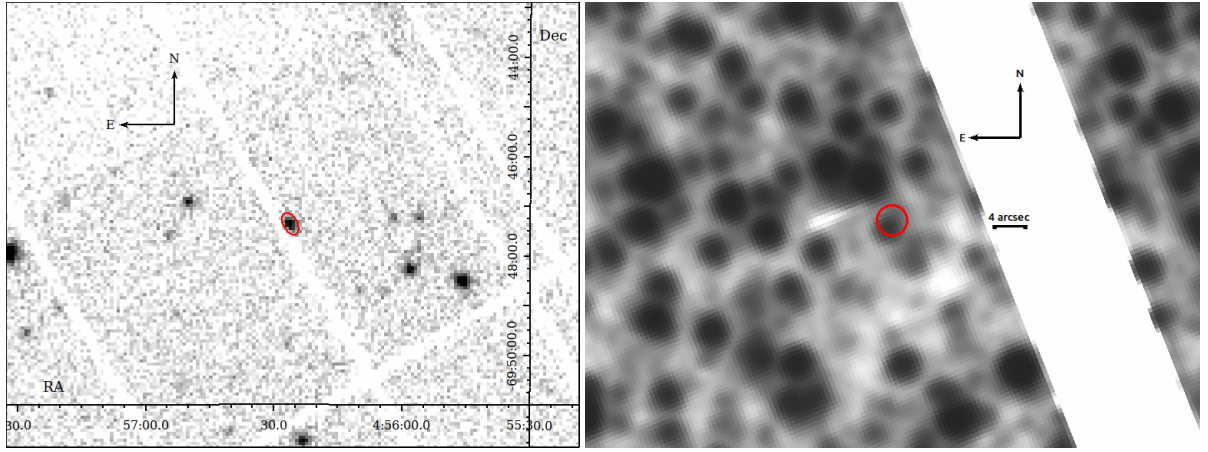


Figure 1. Close-up view of the *XMM-Newton* (left panel) and *SALT* (right panel) field of view, obtained during obs. 0841660501 and the night of the 24 November, 2022, respectively. Note the difference in scale between the two images. The *XMM-Newton* image shows both PN and MOSs data and the source region considered for the events extraction in red. The PN chip border is visible on the left of the source. The *SALT* image shows the J0456 position with the associated error at the 3σ level in red. The white gap on the right is due to the CCD border.

us to extract the events by using an elliptical region with the major axis aligned to the chip edge. The choice of an *ad hoc* region for the extraction was also motivated by the fact that, given the peculiar position of the source, the EXTraS automatic pipeline failed to determine the best circular extraction region.

In Fig. 2 we report the 0.3–10 keV PSD of the PN (top panel) and MOSs (bottom panel) data, together with the 3.5σ detection threshold. The peak is detected in the time series of the three EPIC instruments and not in the event lists of the other sources detected in the field of view. Moreover, no significant peaks are detected in the background regions extracted in different parts of the CCDs. Correspondingly, we can exclude that the detected signal is spurious or due to noise fluctuations. Within the combined PN+MOSs PSD the peak has a significance of 11.3σ (computed over the whole $2 \times 10^{-5} - 0.185$ Hz PSD). The PSD shows no sign of red-noise variability, with a 3σ upper limit on the rms fractional variation of 0.36 from 10 μ Hz up to 10 mHz.

We refined the period estimate through epoch folding (Leahy et al. 1983) and phase-fitting techniques and obtained a value of the period of $P_{\text{spin}} = 7.25243 \pm 0.00004$ s. We derived a 3σ upper limit on its first derivative $|\dot{P}_{\text{spin}}| < 2.1 \times 10^{-8} \text{ s s}^{-1}$. The 0.3–10 keV background-subtracted folded profile is shown in Fig. 3 (bottom curve with filled circle markers) and has a pulsed fraction (defined as the semi-amplitude of the sinusoid divided by the source average count rate) of $PF = (86 \pm 6)\%$. No higher harmonics are needed to fit the profile well. We also considered two sub-bands, 0.3–2 keV and 2–10 keV (chosen so that about half of the events fall in each energy interval), to investigate the dependence of the signal shape as a function of energy. In Fig. 3 we also report the folded profile in the soft (triangle markers, central curve) and hard (diamond markers, top curve) bands, where the pulsed fractions are $PF_{\text{soft}} > 88\%$ (1σ lower limit) and $PF_{\text{hard}} = (85 \pm 10)\%$, respectively. Even in these two cases, the inclusion of higher harmonics in the model did not significantly improve the fit. The hard and soft pulsed fractions are consistent, within 3σ , with each other and with the same, 100% pulsed fraction. Note that all pulse minima are consistent with having zero counts.

For our timing analysis we also considered two RXTE pointings (ObsID 40087-04-01-00 and 96441-01-01-00) during which the J0456 position was covered. We searched for signals around

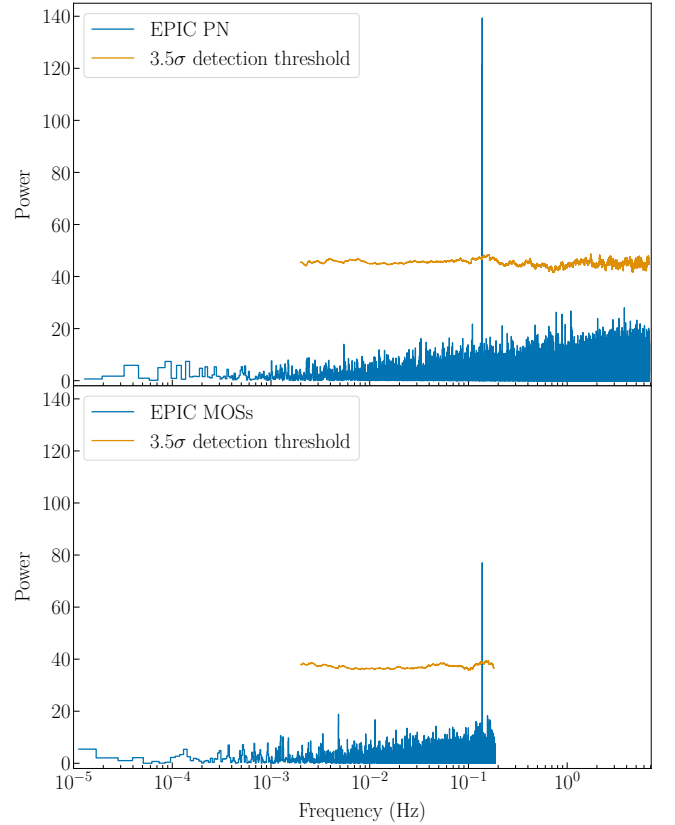


Figure 2. PSD (blue) of J0456 light curve in the 0.3–10 keV band obtained from EPIC PN (top panel) and MOSs (bottom panel) data of observation 0841660501, together with the local 3.5σ detection threshold (orange). The peak at frequency $\nu \approx 0.138$ Hz has a significance of 11.3σ over the whole PN+MOSs PSD.

the *XMM-Newton* detected period (we adopted a maximum $|\dot{P}_{\text{spin}}| < 10^{-10} \text{ s s}^{-1}$) in the Proportional Counter Array (PCA, Jahoda et al. 2006) data, without success. No reliable upper limit on the pulsed fraction could be inferred, being the PCA a non-imaging

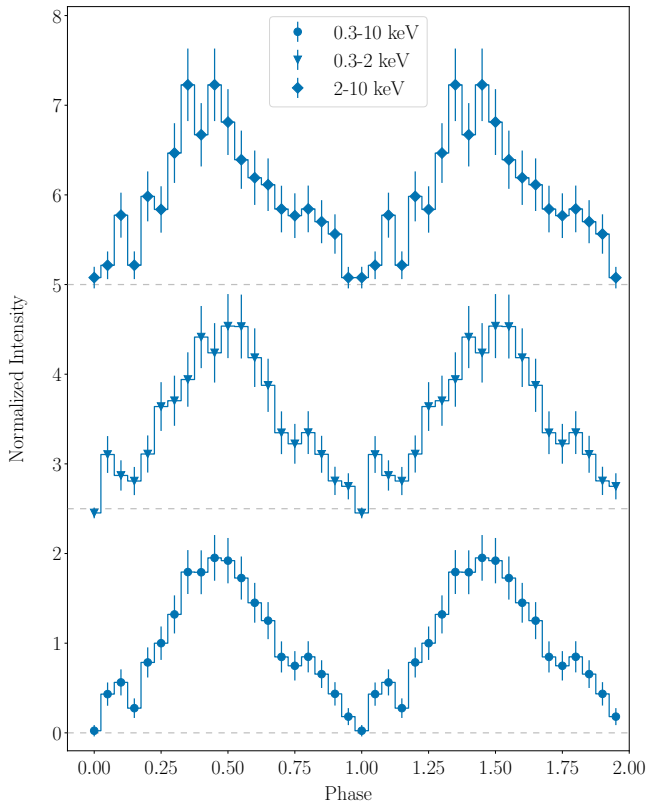


Figure 3. Phase-folded profile of the PN+MOSs background-subtracted light curves in the 0.3–10 keV (circles), 0.3–2 keV (triangles) and 2–10 keV (diamonds) bands. For display purposes, the 0.3–2 keV and 2–10 keV light curves are vertically shifted with an offset equals to 2.5 and 5, respectively. The gray dashed lines show the zero-flux level for each energy band.

instrument, in which the background contribution to the count rate could not be reliably quantified.

3.2 Spectral Analysis

We performed the spectral analysis of J0456 with the *xSPEC* package (Arnaud 1996) v.12.12.0g, which is included in the *HEASOFT*² distribution (v.6.29c). We grouped by three the single bins (to cope with the original spectral resolution) and grouped the data so as to have at least 15 counts in a single spectral bin (to enable a reliable usage of the χ^2 statistics). Different rebinning factors (e.g., 20 counts per bin at least) did not significantly alter the estimated values of the parameters, but we chose a 15-count configuration because it provided a lower uncertainty on the absorption column to the source. The abundances and cross sections were set to those of Wilms et al. (2000) and Verner et al. (1996), respectively. In this section, the uncertainties indicate a 90% confidence range.

We first considered a simple absorbed power-law (PL) model, with two absorption components to account for both the Galactic and the inter-galactic plus LMC absorption: in *xSPEC* syntax, this model corresponds to `tbabs*tbvarabs*powerlaw`. We set the first absorption component (`tbabs`) to the Galactic value³

² <https://heasarc.gsfc.nasa.gov/docs/software/lheasoft/>.

³ Computed by means of NASA’s HEASARC N_{H} web calculator <https://heasarc.gsfc.nasa.gov/cgi-bin/Tools/w3nh/w3nh.pl>.

$N_{\text{H,gal}} = 8.91 \times 10^{20} \text{ cm}^{-2}$ in the direction of the LMC (Dickey & Lockman 1990). Following Haberl et al. (2022b, 2023b) we set the elemental abundances of the LMC `tbvarabs` component at 0.49 times that of the Solar abundance, and allowed the column density to vary. The PL model provides an excellent description of the spectrum ($\chi_r^2 \sim 1$). The associated best-fit parameters are reported in Table 1.

We also considered a model with an additional black body (BB) component, since an absorbed BB+PL is often used to fit the spectra’s of both magnetars and accreting X-ray sources. The addition of a BB component to the PL model did not significantly improve the fit, resulting in a by-chance probability (computed by means of the F-test) of $\approx 1\%$, which led us to discard the model. We also considered an absorbed BB+BB model, since it is often used to fit the magnetars’ spectra (see, e.g., Israel et al. 2016). Our BB+BB model also provides a good description of the observed spectra, with $\chi_r^2 \sim 0.89$, and the values for the temperatures $kT_{\text{BB}} (\approx 0.3$ and 0.9 keV, respectively) and radii $R_{\text{BB}} (\approx 2$ and 0.4 km, respectively) of both BBs are consistent with the ones expected from hotspots on a NS. However, we favored the PL model given its greater simplicity, since it involves one emission component instead of two while still providing a good description of the spectrum. Both the best-fit parameters of the BB+PL and BB+BB model can be found in Table 1. We also tested a single component BB model, but the fit is significantly worse, as shown by a large $\chi_r^2 \sim 1.5$.

The PN and MOSs spectra, together with the best-fit PL model, are shown in Fig. 4. The intrinsic $N_{\text{H}} \approx 4.8 \times 10^{21} \text{ cm}^{-2}$ we derived by adopting the PL spectral model is consistent with the source being of extragalactic origin and the only known system along the line of sight is the LMC. Assuming a distance of 50 kpc for the LMC (Pietrzyński et al. 2013) and correcting for the total absorption, we derive an unabsorbed luminosity of about $L_{\text{X}} \approx 2.7 \times 10^{34} \text{ erg s}^{-1}$ in the 0.3–10 keV band.

For those observations in which J0456 was not detected we computed the 3σ upper limit on its count rate by means of the *sosta* tool in *XIMAGE*⁴. Exploiting the best-fit parameters reported in Table 1 for the PL model, we converted the 3σ upper limits on the count rate in 3σ upper limits on the unabsorbed flux of J0456 in the 0.3–10 keV band⁵. Most *Swift* pointings lasted less than 300 s, too short to derive meaningful upper limits. From the longest observation (obs. 00033492002, $T \approx 630$ s, October 2014) we derived a 3σ upper limit on the unabsorbed flux $F_{\text{X}} = 9.2 \times 10^{-13} \text{ erg cm}^{-2} \text{ s}^{-1}$. The two most stringent upper limits come from the first *XMM-Newton* pointing (obs. 0823790301, May 2018) and *eROSITA* (May and November 2021, May and November 2022). We derived a 3σ upper limit on the count rate in the EPIC-MOS cameras of 9×10^{-4} counts/s, corresponding to a 3σ upper limit on the unabsorbed flux $F_{\text{X}} = 1.5 \times 10^{-14} \text{ erg cm}^{-2} \text{ s}^{-1}$. In the latter, considering the first four *eROSITA* all-sky surveys (eRASS1-4), the derived 3σ upper limit for the unabsorbed flux is $F_{\text{X}} = 3.8 \times 10^{-14} \text{ erg cm}^{-2} \text{ s}^{-1}$ for each survey (F. Haberl, private communication).

3.3 Optical Analysis

High-quality spectra were obtained in the 3800–5850 Å range for the optical object consistent with the X-ray position and are shown in Fig. 5. The red-end of the spectrum (wavelength $\lambda > 5850$ Å)

⁴ <https://heasarc.gsfc.nasa.gov/xanadu/ximage/>.

⁵ All the upper limits have been computed using the WebPIMMS tool: <https://heasarc.gsfc.nasa.gov/cgi-bin/Tools/w3pimms/w3pimms.pl>.

Table 1. Best-fit parameters of the models considered for the phase-averaged spectrum of J0456. PL: power-law component. BB: black body component. Γ : power-law photon index. The reported errors show the 90% confidence region. When only one black body component was adopted in the model we reported the temperature kT_{BB} and the radius R_{BB} under the cold ones column ($kT_{\text{BB}}^{\text{cold}}$ and $R_{\text{BB}}^{\text{cold}}$).

Model	N_{H}^a (10^{21} cm^{-2})	Γ	$kT_{\text{BB}}^{\text{cold}}$ (keV)	$R_{\text{BB}}^{\text{cold}}$ (km)	$kT_{\text{BB}}^{\text{hot}}$ (keV)	$R_{\text{BB}}^{\text{hot}}$ (km)	F_X^b ($10^{-14} \text{ erg cm}^{-2} \text{ s}^{-1}$)	L_X^c ($10^{34} \text{ erg s}^{-1}$)	χ^2/dof
PL	$4.8^{+2.5}_{-2.0}$	$1.93^{+0.23}_{-0.21}$	–	–	–	–	$6.10^{+0.73}_{-0.71}$	$2.73^{+0.45}_{-0.33}$	40.03/40
BB + BB	$< 1.2^d$	–	$0.30^{+0.10}_{-0.09}$	$1.9^{+3.2}_{-1.5}$	$0.86^{+0.18}_{-0.14}$	$0.43^{+0.28}_{-0.40}$	$5.27^{+0.55}_{-0.66}$	$1.58^{+0.17}_{-0.20}$	33.68/38
PL + BB	$< 2.9^d$	$1.4^{+1.2}_{-0.5}$	$0.63^{+0.26}_{-0.12}$	$0.63^{+0.53}_{-0.56}$	–	–	$5.87^{+0.84}_{-0.82}$	$1.9^{+1.0}_{-0.2}$	31.80/38

Notes.

^a The Galactic absorption component was fixed to $N_{\text{H,gal}} = 8.91 \times 10^{20} \text{ cm}^{-2}$ (Dickey & Lockman 1990).

^b Absorbed flux in the 0.3–10 keV band.

^c Unabsorbed luminosity in the 0.3–10 keV band, assuming a distance of 50 kpc.

^d 90% confidence level upper limit.

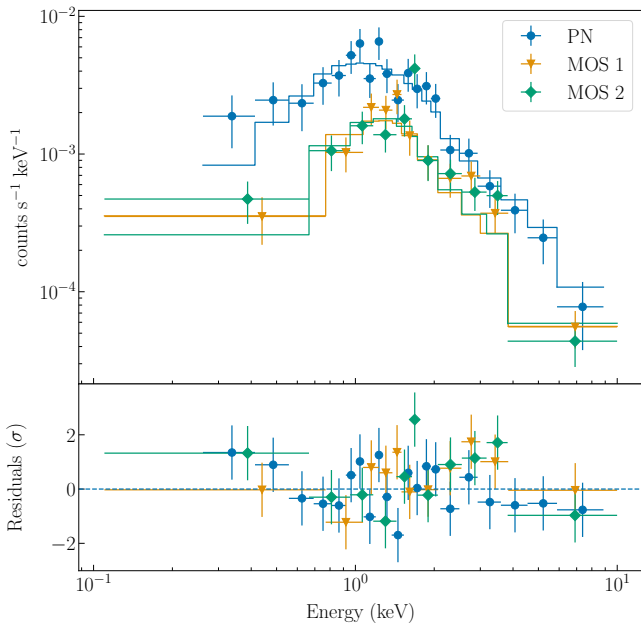


Figure 4. Top: EPIC spectrum of J0456 from observation 0841660501 (blue circles: PN data; yellow triangles: MOS 1 data; green diamonds: MOS 2 data), together with the best-fit absorbed power-law model (same color scheme). Bottom: fit residuals in units of standard deviation (same color and marker scheme as above).

was dominated by diffuse emission of the surroundings during both nights. Therefore, we did not consider this range for our analysis. We derived a relative magnitude of $V \sim 18.9$ mag.

No emission lines usually associated with X-ray reprocessing by the companion and/or an accretion disc, such as the Balmer lines and He II (4686 Å), are found in the spectra. We first checked that the wavelengths of the few absorption lines present in the spectra are shifted by an amount equivalent to a radial velocity of $v_r \sim 250$ km/s ($\Delta\lambda \sim 3.2 - 4.9$ Å in the 3800–5850 Å range), which is consistent with the star being in the LMC (Piatti et al. 2018). Therefore, we associate this star with the LMC. Assuming a distance modulus $\mu \sim 18.5$ mag for the LMC (Subramanian & Subramanian 2013) and an

extinction coefficient⁶ $A_V \sim 0.2$ mag (Schlafly & Finkbeiner 2011), the absolute magnitude in V-band for this star is $M_V \sim 0.2$ mag. This excludes any O or B spectral type star. The optical spectra, in particular, show the Ca II K line at 3933 Å and the Ca II H + He blend at 3969 Å, together with the CH G-band at 4300 Å, the Fe I at 4383 Å and the Mg I triplet at 5167, 5172 and 5183 Å (all the absorption lines are reported to their restframe wavelengths). For our classification we considered spectral features that were visible in both observations. For instance, the lines at 4100–4150 Å, which appeared in emission during the first night (blue spectrum) and in absorption during the second night (yellow spectrum), were excluded as they probably arose from incorrect background subtraction. We can exclude that the source is a late-F star by the absence of lines such as H γ (4340 Å), H8 (3889 Å) and H9 (3835 Å). The spectral shape, absolute magnitude M_V and identified lines are all consistent with the source being a late-type G (G8) or early-type K (K0–3) star of luminosity class III.

4 DISCUSSION

The 7.25-s coherent period of the pulsations strongly suggests that J0456 is a spinning NS. However, the data currently available for J0456 are not sufficient for an unambiguous classification. In fact, without a further measurement of the spin period P_{spin} it is not possible to derive its secular first derivative \dot{P}_{spin} and therefore to determine whether the pulsar is isolated (spin-down) or in an accreting binary system (spin-up). Therefore, we attempted a classification of the source based on the available information from the observations we analysed in the previous section and the MCs environment. J0456 may be identified as either (i) an accreting X-ray pulsar with a G8-K3 III companion or (ii) an isolated NS of the magnetar class.

Concerning the first scenario, we note that we do not have any information on the X-ray activity state of the source at (or around) the time of the optical observations of J0456. Therefore, the absence of the optical emission lines, characteristic of X-ray reprocessing, does not rule out the accreting scenario, as J0456 could be a transient binary system in quiescence at the time of the *SALT* observations.

Given that no LMXB X-ray pulsars are known in the MCs, we

⁶ Computed with the NASA/IPAC Extragalactic Database (NED) Extinction Calculator available online at https://ned.ipac.caltech.edu/extinction_calculator.

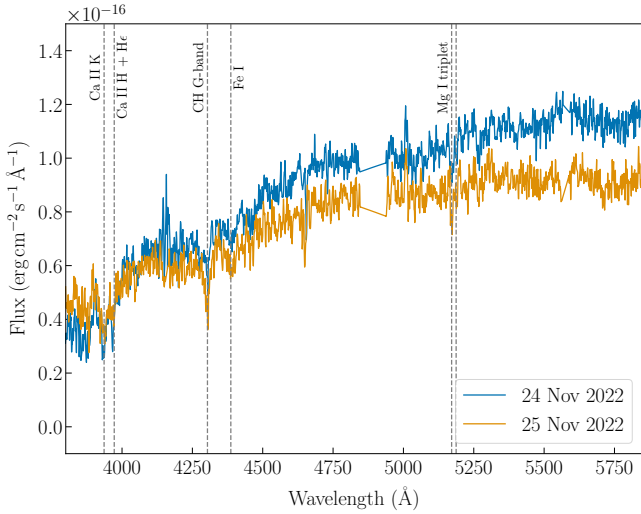


Figure 5. Optical spectra in the 3800–5850 Å band of the candidate optical counterpart of J0456 during the first (blue) and second (yellow) night of observations. The features in the spectra we used for our classification are marked by the gray dashed lines.

started considering the properties of the known X-ray pulsars in the MCs, i.e. those in HMXBs, under the hypothesis that they are coeval with J0456. Christodoulou et al. (2016) presented an analysis on all accreting X-ray pulsars with $P_{\text{spin}} < 10^3$ s in both the LMC and the SMC. By looking at the relation between the minimum X-ray luminosity L_X shown by these sources and their spin periods P_{spin} and following Stella et al. (1986), they were able to derive a typical lower limit on the magnetic field $B > 3 \times 10^{11}$ G for NSs with $P_{\text{spin}} < 15$ s. Assuming that J0456 is an accreting NS we can use the standard expression to derive the corotation radius R_{co}

$$R_{\text{co}} = \left(\frac{GM_{\text{NS}}}{\Omega^2} \right)^{1/3} \approx 1.5 \times 10^8 \left(\frac{M_{\text{NS}}}{M_{\odot}} \right)^{1/3} P^{2/3} \text{ cm} \quad (1)$$

and the magnetospheric radius R_m

$$R_m = 3.3 \times 10^7 \xi_{0.5}^{4/7} L_{39}^{-2/7} R_6^{10/7} M_{1.4}^{1/7} \text{ cm}, \quad (2)$$

where the X-ray luminosity L , the magnetic field B , the radius R of the NS and its mass M are in 10^{39} erg s $^{-1}$, 10^{12} G, 10^6 cm and $1.4M_{\odot}$ units, respectively. In our case $P \approx 7.25$ s, $L_X \approx 2.7 \times 10^{34}$ erg s $^{-1}$. Assuming a standard value for $M_{\text{NS}} \approx 1.4M_{\odot}$, we derived $R_{\text{co}} \approx 6.3 \times 10^8$ cm. In order to have accretion onto the NS $R_m < R_{\text{co}}$. Assuming $\xi = 0.5$, we find that the magnetic field of J0456 should be $B < 9.1 \times 10^{11}$ G. Moreover, assuming that the non detection of the pulsar at a luminosity level a factor of about 4 lower ($L_X \approx 6.7 \times 10^{33}$ erg s $^{-1}$) is related to the onset of the propeller phase, it converts to a magnetic field lower limit of $B > 4.5 \times 10^{11}$ G. Both limiting values are consistent with those obtained by Christodoulou et al. (2016), suggesting that the assumed coeval hypothesis is likely reliable.

Only two LMXBs are known in the MCs. eRASStJ040515.6-745202 (Haberl et al. 2023a) showed a Type-I X-ray burst, indicative of low ($B \lesssim 10^8$ G) magnetic fields, and is not pulsating. LMC X-2, likewise non-pulsating, shows a blue optical spectrum and it is a persistent source (see Lavagetto et al. 2008; Agrawal & Misra 2009; Agrawal & Nandi 2020, and references therein). Few Galactic LMXBs, such as Her X-1, GRO J1744-28, IGR J16358-4726, 3XMM J181923.7-170616 and Swift J1843.5-0343, host X-ray pul-

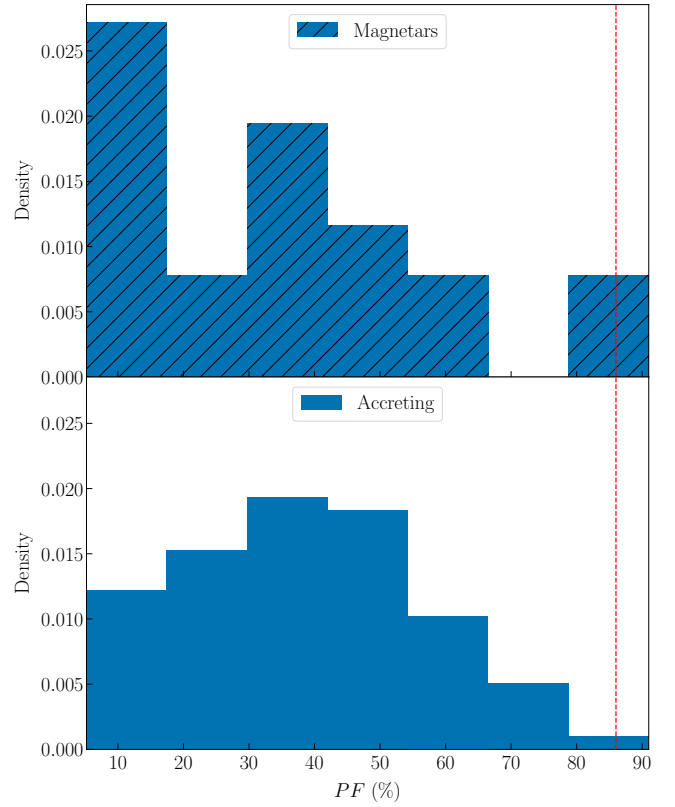


Figure 6. Top panel: distribution of the pulsed fraction of the magnetars reported in the MOOC catalogue (Coti Zelati et al. 2018) at the peak of the outburst. Bottom panel: distribution of the pulsed fraction of the BeXRBs in the MCs during active phases (Coe & Kirk 2015; Antoniou & Zezas 2016; Bartlett et al. 2017; Boon et al. 2017; Haberl et al. 2017; Kennea et al. 2017; Vasilopoulos et al. 2017; Koliopoulos & Vasilopoulos 2018; La Palombara et al. 2018a,b; Maitra et al. 2018, 2021; Carpano et al. 2022; Haberl et al. 2022a,b; Maitra et al. 2023; Haberl et al. 2023b, and references therein) and the pulsars in LMXBs Her X-1, GRO J1744-28, IGR J16358-4726, 3XMM J181923.7-170616 and Swift J1843.5-0343. For these last sources, we refer to the LMXBs XRBCat (Avakyan et al. 2023) and references therein. In both panels the red dashed line marks the pulsed fraction of the signal found in J0456 flux.

sars with similarly high ($B \gtrsim 10^{11}$ G) magnetic fields, though they represent an exception among LMXBs. In fact, the greatest part of known pulsars in LMXBs are usually old NSs spun-up to ms-long spin periods by accretion and, therefore, possess low magnetic fields $B \lesssim 10^8$ G (Bahramian & Degenaar 2022), inconsistent with our findings. Furthermore, the latter class of LMXBs very often shows aperiodic variability in the form of non-Poissonian power spectrum noise components (likely originated by the accretion process itself). The latter is simply not detected in the *XMM-Newton* dataset (see the PSD shown in Fig. 2). Note that, following the recently released LMXB Cat⁷ (Avakyan et al. 2023), for our discussion we included the symbiotic X-ray binaries (SyXBs, XRBs composed of an accreting NS and a late-type K1-M8 companion; see Tab. 1 in Yungelson et al. 2019 for a list of confirmed and candidates SyXBs) among the LMXBs. Summarizing, within the accreting X-ray pulsar scenario, J0456 might be a new member of the rare class of relatively

⁷ <http://astro.uni-tuebingen.de/~xrbcat/> and references therein.

young pulsars in LMXBs/SyXBs, the first ever in the MCs, with very peculiar properties.

The XRB scenario is also challenged by a previous work of [Antoniou & Zezas \(2016\)](#). Starting from the LMC star formation history reconstructed by [Harris & Zaritsky \(2009\)](#) and the data coming from the Magellanic Clouds Photometric Survey (MCPS, [Zaritsky et al. 2004](#)), they estimated the chance coincidence probability for an optical source to be found in the uncertainty region of an X-ray source in the LMC as a function of both the absolute magnitude M_V and the reddening-corrected color index $B - V$. As one can see from Fig. 2 in the original paper, for a source with $M_V \sim 0.2$ mag like ours this probability is always $\geq 62\%$ within a 5 arcsec region. Their results are probably (at least partially) driven by the fact that they included the central region of the LMC, where more massive (O/B-type) stars are expected. Even considering this effect and the fact that they considered a bigger uncertainty region than us, we expect this probability to be only a factor of few higher than the chance coincidence probability for J0456, especially considering how crowded the *SALT* field is (as can be seen in Fig. 1).

It is worth noticing that a period of 7.25-s might be still compatible with the spin period of an accreting white dwarf (WD). For example, the fastest-spinning accreting WDs, i.e. AE Aqr, LAM-OST J024048.51+195226.9 (though X-ray quiet) and HD 49798⁸, show a spin period of about 33 ([Li et al. 2016](#)), 25 ([Pelisoli et al. 2022](#)) and 13 s ([Israel et al. 1997](#)), respectively. Correspondingly, in the accreting WD scenario J0456 might be associated to an intermediate polar (IP) systems similar to those above cited. If so, J0456 would be simultaneously the fastest and brightest (typical luminosities⁹ are $L_X \lesssim 10^{32} - 10^{33} \text{ erg s}^{-1}$) accreting WD of the whole IP class, the first ever in the MCs. The lack of orbital modulation in the spin signal phase is also an indication that, if J0456 were an accreting source, the orbital period should be at least 3–4 times the duration of the observation ($T \approx 47$ ks). This corresponds to $P_{\text{orb}} \geq 40$ h, the second longest orbital period for an IP after GK Per (with an orbital period of ~ 2 d, [Álvarez-Hernández et al. 2021](#)), if not longer. Finally, IPs often show strong optical emission lines both during quiescence and active phases ([Saito et al. 2010](#)). Our *SALT* spectra, on the other hand, do not show similar features. On the light of these factors, we consider this scenario rather unlikely. We also took into account the possibility of an isolated (non-accreting) WD like AR Sco ([Takata et al. 2018](#)). However, J0456 is 4 orders of magnitude brighter than AR Sco and the alternation active-quiescent phases is not expected in isolated sources. Therefore, we consider this scenario unlikely too.

If J0456 is not associated with the G8-K3 III star, it might be related to the other class of variable NSs observed in the MCs, e.g. magnetars. In order to further explore this scenario we compared the source X-ray luminosity L_X in the 0.3–10 keV band and the spin period P_{spin} with the ones shown by all the magnetars included in the Magnetar Outburst Online Catalogue¹⁰ ([Coti Zelati et al. 2018](#)). We also compared them with the same quantities shown by the BeXRBs in the SMC and the LMC for which both L_X and P_{spin} measurements were available during active phases. We considered the BeXRBs reported by [Coc &](#)

[Kirk \(2015\)](#) for the SMC and [Antoniou & Zezas \(2016\)](#) for the LMC. We then cross-checked our sample in the Bologna INAF/IAPS catalogue of accreting X-ray binaries¹¹ to check for missing pulsars not included in the aforementioned catalogues/publications. To convert the flux in luminosity we considered a distance of 50 kpc ([Pietrzyński et al. 2013](#)) and 62 kpc ([Graczyk et al. 2014](#)) for the LMC and SMC, respectively. We also included the same quantities for the few Galactic high-B X-ray pulsars found in LMXBs. Since J0456 has been detected only once, we probably observed the source during a period of high activity. In order to compare these sources with J0456, we considered their L_X and P_{spin} values as inferred during their outburst peak (in the case of magnetars) or during their high luminosity phases (in the case of BeXRBs and LMXBs). We considered the persistent luminosity values for those magnetars for which we do not have detection of an outburst: 1E 1841-045 ([Vasisht & Gotthelf 1997](#)), SGR 1900+14 ([Mereghetti et al. 2006](#)), 4U 0142+614 ([Rea et al. 2007b](#)), 1RXS J170849.0-490910 ([Rea et al. 2007a](#)), CXOU J010043.1-721134 ([McGarry et al. 2005](#)), CXOU J171405.7-381031 ([Gotthelf et al. 2019](#)) and SGR 0526-66 ([Mazets et al. 1979](#)). Finally, for the LMXBs (often showing large flux ranges) we assumed average values of the fluxes, while we assumed the mean distance reported by the LMXB Cat to convert the flux in luminosity.

J0456 is a peculiar case where both a short P_{spin} and low L_X are observed, a combination typically associated with magnetars only. Indeed, the magnetars in our sample are found to have a luminosity $L_X \approx 10^{34} - 10^{36} \text{ erg s}^{-1}$. Accreting X-ray pulsars at similar (~ 7 s) periods, instead, show a luminosity which is at least one order of magnitude higher ($\sim 10^{35} \text{ erg s}^{-1}$), with the least luminous XRBs at these periods in the MCs being LXP 8.04 at $L_X \approx 1.5 \times 10^{35} \text{ erg s}^{-1}$ ([Vasilopoulos et al. 2014](#)) and SXP 7.92 at $L_X \approx 1 \times 10^{36} \text{ erg s}^{-1}$ ([Bartlett et al. 2017](#)).

A second indication of the magnetar nature of J0456 comes from spectral analysis. As already explained in Sect. 3.2, a simple power-law (PL) model was enough to obtain a good fit of the energy spectrum. Although both accreting X-ray pulsars and magnetars can exhibit a power-law component in their spectra, a photon index $\Gamma \approx 1.9$ is particularly high for an accreting system. A photon index $\Gamma \sim 2$, instead, is in line (although not particularly high) with the values usually found for transient magnetars ([Esposito et al. 2021](#)). It is also interesting to note that in the BB+BB model, often employed to describe magnetars' emission in outburst, the radii and temperatures associated with the BBs would be $R \approx 2$ km and 0.4 km and $kT_{\text{BB}} \approx 0.3$ keV and 0.9 keV, respectively. Both values are compatible with those found for other magnetars (see [Esposito et al. 2021](#), and references therein). In this magnetar scenario, the dipolar magnetic field is expected to be of the order of 10^{14} G.

We further note that high-amplitude pulsed fractions are more common in magnetars than in accreting pulsars. Fig. 6 shows the distribution of *PF*s for the magnetars (blue barred histogram in the top panel) and BeXRBs+LMXBs (blue histogram in the bottom panel) in our sample compared to the *PF* inferred for J0456 (red dashed line). For the *PF* we considered the value shown during an outburst/high-active phase as for L_X and P_{spin} . At $PF > 80\%$ (the range of interest for J0456) the probability of finding an XRB with properties similar to those of J0456 is rather low, while it is not negligible for magnetars. Indeed, 2 out of the 21 magnetars in our sample show a pulsed fraction $PF > 80\%$, while only one XRB, SXP95.2 ([Laycock et al. 2002](#)), out of 80 shows such a high pulsed

⁸ Although the nature of HD 49798 is still debated, a recent work by [Mereghetti et al. \(2021\)](#) supports an accreting WD scenario.

⁹ See the IP catalog <https://asd.gsfc.nasa.gov/Koji.Mukai/iphome/catalog/alpha.html> and references therein.

¹⁰ An online and updated version of this catalogue can be found in the Magnetar Outburst Online Catalogue (MOOC): <http://magnetars.ice.csic.es/#/welcome>. A catalogue of known magnetars has been compiled also by [Olausen & Kaspi \(2014\)](#) and an updated version can be found at <http://www.physics.mcgill.ca/~pulsar/magnetar/main.html>.

¹¹ http://www.iasfbo.inaf.it/~mauro/pulsar_list.html and references therein.

fraction. We also note that J0456 pulse profiles in Fig. 3 show a minimum consistent with a null flux, which is hard to explain in the framework of an accreting X-ray source, where low amplitude modulations are expected due to the presence of the accretion disc. There are no X-ray pulsars in the MCs with average pulse minima consistent with a zero flux level. In the case of isolated NSs, on the other hand, a zero-flux level can be easily explained in terms of geometrical occultation of an emitting region in the proximity of the surface by the NS itself.

Finally, the $(L_X, P_{\text{spin}}, PF)$ combination shown by J0456 is very similar to that of the magnetar 1E 1048.1-5937. Tiengo et al. (2005) reported for this source $P_{\text{spin}} \approx 6.46$ s, $PF \approx 91\%$ at a luminosity level of $L_X \approx 2.23 \times 10^{34}$ erg s⁻¹ during *XMM-Newton* obs. 0112780401 (Observation A in Tiengo et al. 2005). Moreover, the spectral parameters they derived for the black bodies in the PL+BB and BB+BB models (first two models in Tab. 2 of the original article) are consistent with the ones we find for J0456 in our spectral analysis. In particular, in the BB+BB model for the hot (cold) component they derive $R_{\text{BB}} \approx 0.3$ km (1.7 km) and $kT_{\text{BB}} \approx 1$ keV (0.5 keV, see Observation A in Tab. 2 of Tiengo et al. 2005).

5 CONCLUSIONS

We have reported on the discovery of a 7.25-s pulsar in the outskirts of the LMC, 4XMMJ045626.3-694723 (J0456). Based on *SALT* optical observations, we conclude that the only stellar object present within the X-ray uncertainty region is a faint, late-type (G8-K3 III) star. We discussed two scenarios for J0456: an accreting NS in a binary system with a late-type star companion (the first in the MCs) or an isolated NS, likely of the magnetar class.

When comparing the J0456 properties with those BeXRBs in the MCs and a few known Galactic X-ray pulsars in LMXBs/SyXBs with a similarly high magnetic field, the 0.3–10 keV luminosity $L_X \approx 2.7 \times 10^{34}$ erg s⁻¹ of J0456 is too low for an accreting NS spinning at ~ 7.25 s and with the magnetic field strength reported above. Moreover, the pulsed fraction of the signal $PF \approx 86\%$ (with pulse minima consistent with null X-ray flux) is rarely observed in any accreting NS considered in our sample (see Fig. 6). All these findings together make the accretion scenario unlikely. Nonetheless, if the accreting nature of J0456 were confirmed, it would represent the outcome of a novel evolutionary path in the MCs.

On the other hand, the characteristics of J0456 (L_X , PF and P_{spin}) are more commonly found in magnetars. In particular, another transient magnetar, 1E 1048.1-5937, shows a very similar spin period $P_{\text{spin}} \approx 6.46$ s and similar pulsed fraction ($\approx 91\%$) at low luminosities $L_X \sim 2 \times 10^{34}$ erg s⁻¹ (Tiengo et al. 2005). If the new pulsar were a magnetar, it would represent the third known magnetar outside our galaxy and the second in the LMC.

An unambiguous classification of the new pulsar is complicated by the lack of a second measurement of the spin period which would have allowed us to infer the first derivative \dot{P}_{spin} of the spin period. Although our findings point to a new member of the magnetar class, we cannot totally exclude, at this stage, the possibility that the source is a peculiar accreting NS in a LMXB/SyXB. Future observations are needed in order to classify J0456.

ACKNOWLEDGEMENTS

This work has made use of the XRT Data Analysis Software (XRT-DAS) developed under the responsibility of the ASI Science Data

Center (ASDC), Italy. The optical observations reported in this paper were obtained with the Southern African Large Telescope (*SALT*). The *SALT* observations were obtained under the *SALT* Science Programme on the characterisation of the optical counterpart of the newly discovered pulsar (2022-2-SCI-012; PI: M.I.). This work has made use of data from the European Space Agency (ESA) mission *Gaia* (<https://www.cosmos.esa.int/gaia>), processed by the *Gaia* Data Processing and Analysis Consortium (DPAC, <https://www.cosmos.esa.int/web/gaia/dpac/consortium>). Funding for the DPAC has been provided by national institutions, in particular the institutions participating in the *Gaia* Multilateral Agreement. This work is based on data from eROSITA, the soft X-ray instrument aboard SRG, a joint Russian-German science mission supported by the Russian Space Agency (Roskosmos), in the interests of the Russian Academy of Sciences represented by its Space Research Institute (IKI), and the Deutsches Zentrum für Luft- und Raumfahrt (DLR). The SRG spacecraft was built by Lavochkin Association (NPOL) and its subcontractors, and is operated by NPOL with support from the Max Planck Institute for Extraterrestrial Physics (MPE). The development and construction of the eROSITA X-ray instrument was led by MPE, with contributions from the Dr. Karl Remeis Observatory Bamberg & ECAP (FAU Erlangen-Nuernberg), the University of Hamburg Observatory, the Leibniz Institute for Astrophysics Potsdam (AIP), and the Institute for Astronomy and Astrophysics of the University of Tübingen, with the support of DLR and the Max Planck Society. The Argelander Institute for Astronomy of the University of Bonn and the Ludwig Maximilians Universität Munich also participated in the science preparation for eROSITA. IRAF was distributed by the National Optical Astronomy Observatory, which was managed by the Association of Universities for Research in Astronomy (AURA) under a cooperative agreement with the National Science Foundation. M.I. is supported by the AASS Ph.D. joint research programme between the University of Rome "Sapienza" and the University of Rome "Tor Vergata", with the collaboration of the National Institute of Astrophysics (INAF). M.I. thanks Dr. Elizabeth Nalunsa for the on-site technical support with the *SALT* observations. G.L.I., P.E., and A.T. acknowledge financial support from the Italian Ministry for University and Research, through grant 2017LJ39LM (UNIAM). F.C.Z. is supported by a Ramón y Cajal fellowship (grant agreement RYC2021-030888-I). F.C.Z. and N.R. are supported by the ERC Consolidator Grant "MAGNESIA" (No. 817661) and are also partially supported by the program Unidad de Excelencia María de Maeztu CEX2020-001058-M. L.S. acknowledges financial contributions from ASI-INAF agreements 2017-14-H.O and I/037/12/0; from "iPesca" research grant (P.I. Andrea Possenti) funded under the INAF call PRIN-SKA/CTA (resolution 70/2016), from PRIN-INAF 2019 no. 15 and from the Italian Ministry of University and Research (MUR), PRIN 2020 (prot. 2020BRP57Z) 'Gravitational and Electromagnetic-wave Sources in the Universe with current and nextgeneration detectors (GEMS)'.

Software: Matplotlib (Hunter 2007), numpy (Harris et al. 2020), pandas (McKinney 2010), SAS (Gabriel et al. 2004), HEASOFT, EX-TraS pipeline (De Luca et al. 2021), IRAF.

DATA AVAILABILITY

The *XMM-Newton* data analysed in this article are public and can be downloaded from the *XMM-Newton* Science Archive XSA (<http://nxsa.esac.esa.int/nxsa-web/#search>) and the High Energy Astrophysics Science Archive Research Center (HEASARC) archive (<https://heasarc.gsfc.nasa.gov/cgi->

bin/W3Browse/w3browse.pl). *SALT* data are available upon request to the authors.

REFERENCES

- Agrawal V. K., Misra R., 2009, *MNRAS*, **398**, 1352
- Agrawal V. K., Nandi A., 2020, *MNRAS*, **497**, 3726
- Álvarez-Hernández A., et al., 2021, *MNRAS*, **507**, 5805
- Antoniou V., Zezas A., 2016, *MNRAS*, **459**, 528
- Antoniou V., Zezas A., Hatzidimitriou D., Kalogera V., 2010, *ApJ*, **716**, L140
- Arnaud K. A., 1996, in Jacoby G. H., Barnes J., eds, *ASPC Vol. 101, Astronomical Data Analysis Software and Systems V*, p. 17
- Avakyan A., Neumann M., Zainab A., Doroshenko V., Wilms J., Santangelo A., 2023, *arXiv e-prints*, p. [arXiv:2303.16168](https://arxiv.org/abs/2303.16168)
- Bahramian A., Degenar N., 2022, *arXiv e-prints*, p. [arXiv:2206.10053](https://arxiv.org/abs/2206.10053)
- Bartlett E. S., Coe M. J., Israel G. L., Clark J. S., Esposito P., D’Elia V., Udalski A., 2017, *MNRAS*, **466**, 4659
- Boon C. M., et al., 2017, *MNRAS*, **466**, 1149
- Buckley D. A. H., Swart G. P., Meiring J. G., 2006, in Stepp L. M., ed., *SPIE*, p. 62670Z, [doi:10.1117/12.673750](https://doi.org/10.1117/12.673750)
- Burgh E. B., Nordsieck K. H., Kobulnicky H. A., Williams T. B., O’Donoghue D., Smith M. P., Percival J. W., 2003, in Iye M., Moorwood A. F. M., eds, *SPIE*, p. 1463, [doi:10.1117/12.460312](https://doi.org/10.1117/12.460312)
- Carpano S., Haberl F., Maitra C., Freyberg M., Dennerl K., Schwobe A., Buckley A. H., Monageng I. M., 2022, *A&A*, **661**, A20
- Chatterjee R., Agrawal V. K., Nandi A., 2021, *MNRAS*, **505**, 3785
- Christodoulou D. M., Laycock S. G. T., Yang J., Fingerma S., 2016, *ApJ*, **829**, 30
- Coe M. J., 2000, *ASPC*, **214**, 656
- Coe M. J., Kirk J., 2015, *MNRAS*, **452**, 969
- Coti Zelati F., Rea N., Pons J. A., Campana S., Esposito P., 2018, *MNRAS*, **474**, 961
- Crawford S. M., et al., 2012, *PySALT: SALT science pipeline*, *Astrophysics Source Code Library*, record ascl:1207.010
- De Luca A., et al., 2021, *A&A*, **650**, 167
- Dickey J. M., Lockman F. J., 1990, *ARA&A*, **28**, 215
- Duncan R. C., Thompson C., 1992, *ApJ*, **392**, L9
- Esposito P., Rea N., Israel G. L., 2021, in Belloni T. M., Méndez M., Zhang C., eds, *Astrophysics and Space Science Library Vol. 461, Timing Neutron Stars: Pulsations, Oscillations and Explosions*. pp 97–142 ([arXiv:1803.05716](https://arxiv.org/abs/1803.05716)), [doi:10.1007/978-3-662-62110-3_3](https://doi.org/10.1007/978-3-662-62110-3_3)
- Gabriel C., et al., 2004, in Ochsenbein F., Allen M. G., Egret D., eds, *ASPC Vol. 314, Astronomical Data Analysis Software and Systems (ADASS) XIII*, p. 759
- Gaia Collaboration et al., 2022, *arXiv e-prints*, p. [arXiv:2208.00211](https://arxiv.org/abs/2208.00211)
- Gotthelf E. V., Halpern J. P., Mori K., Beloborodov A. M., 2019, *ApJ*, **882**, 173
- Graczyk D., et al., 2014, *ApJ*, **780**, 59
- Haberl F., Sturm R., 2016, *A&A*, **586**, A81
- Haberl F., et al., 2017, *A&A*, **598**, A69
- Haberl F., et al., 2022a, *A&A*, **661**, A25
- Haberl F., Maitra C., Vasilopoulos G., Maggi P., Udalski A., Monageng I. M., Buckley D. A. H., 2022b, *A&A*, **662**, A22
- Haberl F., et al., 2023a, *A&A*, **669**, A66
- Haberl F., et al., 2023b, *A&A*, **671**, A90
- Harris J., Zaritsky D., 2009, *AJ*, **138**, 1243
- Harris C. R., et al., 2020, *Nature*, **585**, 357
- Hunter J. D., 2007, *CSE*, **9**, 90
- Israel G. L., Stella L., 1996, *ApJ*, **468**, 369
- Israel G. L., Stella L., Angelini L., White N. E., Kallman T. R., Giommi P., Treves A., 1997, *ApJ*, **474**, L53
- Israel G. L., et al., 2016, *MNRAS*, **457**, 3448
- Jahoda K., Markwardt C. B., Radeva Y., Rots A. H., Stark M. J., Swank J. H., Strohmayer T. E., Zhang W., 2006, *ApJS*, **163**, 401
- Jansen F., et al., 2001, *A&A*, **365**, L1
- Kaspi V. M., Beloborodov A. M., 2017, *ARA&A*, **55**, 261
- Kennea J. A., Evans P. A., Coe M. J., Udalski A., 2017, *ATEL*, **10600**, 1
- Kirsch M., et al., 2004, *SPIE*, **5488**, 103
- Kobulnicky H. A., Nordsieck K. H., Burgh E. B., Smith M. P., Percival J. W., Williams T. B., O’Donoghue D., 2003, in Iye M., Moorwood A. F. M., eds, *SPIE*, p. 1634, [doi:10.1117/12.460315](https://doi.org/10.1117/12.460315)
- Koliopoulos F., Vasilopoulos G., 2018, *A&A*, **614**, A23
- Kulkarni S. R., Kaplan D. L., Marshall H. L., Frail D. A., Murakami T., Yonetoku D., 2003, *ApJ*, **585**, 948
- La Palombara N., Esposito P., Mereghetti S., Pintore F., Sidoli L., Tiengo A., 2018a, *MNRAS*, **475**, 1382
- La Palombara N., Esposito P., Pintore F., Sidoli L., Mereghetti S., Tiengo A., 2018b, *A&A*, **619**, A126
- Lamb R. C., Fox D. W., Macomb D. J., Prince T. A., 2002, *ApJ*, **574**, L29
- Lamb R. C., Fox D. W., Macomb D. J., Prince T. A., 2003, *ApJ*, **599**, L115
- Lavagetto G., Iaria R., D’Aì A., di Salvo T., Robba N. R., 2008, *A&A*, **478**, 181
- Laycock S., Corbet R. H. D., Perrodin D., Coe M. J., Marshall F. E., Markwardt C., 2002, *A&A*, **385**, 464
- Leahy D. A., Darbro W., Elsner R. F., Weisskopf M. C., Sutherland P. G., Kahn S., Grindlay J. E., 1983, *ApJ*, **266**, 160
- Li J., Torres D. F., Rea N., de Oña Wilhelmi E., Papitto A., Hou X., Mauche C. W., 2016, *ApJ*, **832**, 35
- Maitra C., Paul B., Haberl F., Vasilopoulos G., 2018, *MNRAS*, **480**, L136
- Maitra C., Haberl F., Maggi P., Kavanagh P. J., Vasilopoulos G., Sasaki M., Filipović M. D., Udalski A., 2021, *MNRAS*, **504**, 326
- Maitra C., et al., 2023, *A&A*, **669**, A30
- Mazets E. P., Golenetskii S. V., Il’inskii V. N., Aptekar’ R. L., Guryan Y. A., 1979, *Nature*, **282**, 587
- McGarry M. B., Gaensler B. M., Ransom S. M., Kaspi V. M., Veljkovic S., 2005, *ApJ*, **627**, L137
- McKinney W., 2010, in van der Walt S., Millman J., eds, *Proceedings of the 9th Python in Science Conference. Proceedings of the Python in Science Conference. SciPy*, pp 56–61, [doi:10.25080/Majora-92bf1922-00a](https://doi.org/10.25080/Majora-92bf1922-00a)
- Mereghetti S., et al., 2006, *ApJ*, **653**, 1423
- Mereghetti S., et al., 2021, *MNRAS*, **504**, 920
- Okazaki A. T., Negueruela I., 2001, *A&A*, **377**, 161
- Olausen S. A., Kaspi V. M., 2014, *ApJS*, **212**, 6
- Park S., Bhalerao J., Kargaltsev O., Slane P. O., 2020, *ApJ*, **894**, 17
- Pelissoli I., et al., 2022, *MNRAS*, **509**, L31
- Piatti A. E., Hwang N., Cole A. A., Angelo M. S., Emptage B., 2018, *MNRAS*, **481**, 49
- Pietrzyński G., et al., 2013, *Nature*, **495**, 76
- Predehl P., et al., 2021, *A&A*, **647**, A1
- Prusti T., et al., 2016, *A&A*, **595**, A1
- Rea N., et al., 2007a, *Ap&SS*, **308**, 505
- Rea N., et al., 2007b, *MNRAS*, **381**, 293
- Saito R. K., Baptista R., Horne K., Martell P., 2010, *AJ*, **139**, 2542
- Schlaflly E. F., Finkbeiner D. P., 2011, *ApJ*, **737**, 103
- Stella L., White N. E., Rosner R., 1986, *ApJ*, **308**, 669
- Strüder L., et al., 2001, *A&A*, **365**, L18
- Subramanian S., Subramanian A., 2013, *A&A*, **552**, A144
- Takata J., Hu C. P., Lin L. C. C., Tam P. H. T., Pal P. S., Hui C. Y., Kong A. K. H., Cheng K. S., 2018, *ApJ*, **853**, 106
- Tiengo A., Mereghetti S., Turolla R., Zane S., Rea N., Stella L., Israel G. L., 2005, *A&A*, **437**, 997
- Tiengo A., Esposito P., Mereghetti S., 2008, *ApJ*, **680**, L133
- Tiengo A., et al., 2009, *MNRAS*, **399**, L74
- Turner M. J., et al., 2001, *A&A*, **365**, L27
- Turolla R., Zane S., Watts A. L., 2015, *RPPH*, **78**, 116901
- Vasilopoulos G., Haberl F., Sturm R., Maggi P., Udalski A., 2014, *A&A*, **567**, A129
- Vasilopoulos G., Zezas A., Antoniou V., Haberl F., 2017, *MNRAS*, **470**, 4354
- Vasilopoulos G., Maitra C., Haberl F., Hatzidimitriou D., Petropoulou M., 2018, *MNRAS*, **475**, 220
- Vasisht G., Gotthelf E. V., 1997, *ApJ*, **486**, L129
- Verner D. A., Ferland G. J., Korista K. T., Yakovlev D. G., 1996, *ApJ*, **465**, 487
- Webb N. A., et al., 2020, *A&A*, **641**, A136
- Wilms J., Allen A., McCray R., 2000, *ApJ*, **542**, 914

Yungelson L. R., Kuranov A. G., Postnov K. A., 2019, [MNRAS](#), **485**, 851
Zaritsky D., Harris J., Thompson I. B., Grebel E. K., 2004, [AJ](#), **128**, 1606

This paper has been typeset from a \TeX/L\AA\TeX file prepared by the author.